

Analysis of 4-year observations of the gPhone#59 in Tahiti

O. Francis¹, J.-P. Barriot² and D. Reymond³

¹ University of Luxembourg, FSTC, Luxembourg, olivier.francis@uni.lu

² Geodesy Observatory of Tahiti (OGT), University of French Polynesia (UPF), Tahiti, jean-pierre.barriot@upf.pf

³ Laboratory of Geophysics (LDG), French Atomic Energy Agency (CEA), Tahiti, reymond.d@labogeo.pf

Abstract. Since 2009, the relative spring gravimeter gPhone#059 is operating almost continuously in Pamatai, Tahiti. Although Tahiti is an island, the tidal oceanic gravitational attraction and elastic loading effects are relatively moderate. However, the data are affected by a huge microseismic signal. We present the results of the earth tides analysis and compare them with the latest theoretical WDD Earth tides model combined with modeled oceanic loading and attraction effects. The atmospheric pressure regime is unique with a strong semi-diurnal component.

1. Introduction

Tahiti Island ($17^{\circ} 34' S$, $149^{\circ} 36' W$) is part of French Polynesia, a swarm of 120 islands located in the middle of the South Pacific Ocean. It comprises three volcanic edifices: Moorea, Tahiti-Nui and Tahiti-Iti, spread over 100 km (Figure 1). The formation is dated 0.5-1.4 Million years, with an end of the volcanism activities 250,000 years ago (Hildenbrand et al., 2008).

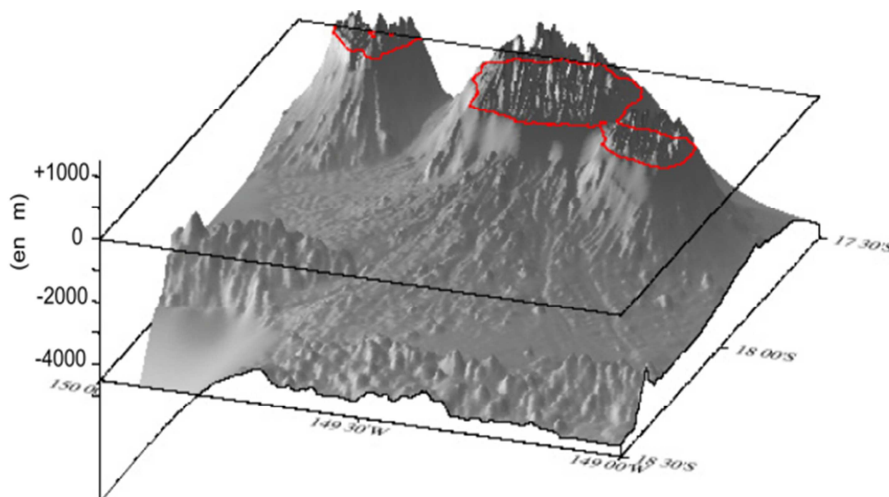


Figure 1. Tahiti islands complex (from left to right: Moorea, Tahiti-Nui and Tahiti-Iti volcanic edifices). Clouard and Bonneville (2003), with permission.

In 2009, the University of French Polynesia acquired the gPhone#59 relative spring gravimeter manufactured by MicrogLaCoste Inc. It was installed in a remote vault with difficult access, next to the GEOSCOPE instruments in Tahiti-Pamatai (Figures 2). Since then, the gravity variations are measured almost continuously. Despite all the care, there are some gaps due to electric power shortages.



Figures 2. Instrument vault in Tahiti-Pamatai (left) and the gPhone#59 with Geoscope broadband seismometers (right) in Tahiti (GPS coordinates: latitude: -17.5896 ; longitude: -149.5625 and altitude: 705 m).

The station is at an altitude of 705 m above the mean sea level at a distance of 5 km from the sea. Despite the proximity to the sea and the high altitude, the tidal oceanic attraction and elastic loading effects are quite reasonable: 1.4 microgal for M_2 and 0.5 microgal for K_1 , respectively. The altitude enhances the magnitude of the gravitational attraction effects of the tidal water around Tahiti (if the altitude was at the same level as the mean sea level, the direct attraction effects would be zero). It means that the quality and the resolution of the ocean tides around Tahiti will play a crucial role to accurately model the oceanic loading and attraction effects.

In this paper, we begin with a short presentation of the gPhone along the results of an assessment of its performance carried out in the Walferdange Underground Laboratory for Geodynamics in Luxembourg. We then describe the observations and the data processing of the gravity observations. The Earth tides analysis results are then presented and discussed. We conclude with some perspectives for future work.

2. The gPhone: a portable Earth tidal spring gravimeter

The gPhone is the last born relative spring gravimeter based on the LaCoste-Romberg meter patented in 1952. The first generation meter had a single oven heating system for thermal stability and a zero length spring. In 2004, MicrogLaCoste Inc. started to redesign and improve the hardware and software components. This includes: a low drift metal zero length spring, a CPI (Capacitance Position Indicator) feedback system, a coarse screw to adjust the spring tension (world-wide gravity range), a linear electronic feedback with a range between 20 to 40 mGal (insuring 2 years operation without adjusting the spring), a double-oven container (very accurate and stable temperature control at 1 mK), an inner oven filled with dry Nitrogen (stable humidity environment), 3 sealed chambers to protect from outside ambient humidity and pressure variation, inner and outer oven chambers thick walled aluminum O-ring sealed and leak tested, outer grey box O-ring sealed for water tightness. Additional and interesting features were added like: a rubidium clock for keeping the time steered by GPS, 1-second data sampling including the long and cross levels, the ambient pressure and temperature, the sensor temperature, the meter inside pressure and the beam position. The gPhone is not designed to be moved around to measure a network of stations as a Scintrex, for example. It is devoted to semi-permanent stations to estimate the tidal parameters and to measure continuously temporal gravity change at a fixed station.

In order to illustrate the performance of the gPhone, the noise power spectral density of four different sensors operating at the same time in the Walferdange Underground Laboratory for Geodynamics is presented in Figure 3. The gPhone has a performance lying between the superconducting gravimeter and the relative spring gravimeter Scintrex CG-5. At short period less than 10 seconds, the signal of the superconducting gravimeter is attenuated by the analog low-passed filter of its electronics. At periods less than 20 seconds, the gPhone and the Streckeisen STS-2 broadband seismometer (for more information about the STS-2 go to the web site <https://www.passcal.nmt.edu/content/instrumentation/sensors/broadband-sensors/sts-2-bb-sensor>) noises are similar. Obviously, the STS-2 can sample the data at much higher frequency than the gPhone. However, the gPhone could be used to calibrate the STS-2. This cannot be done with the superconducting gravimeter because of its low-pass analog filter.

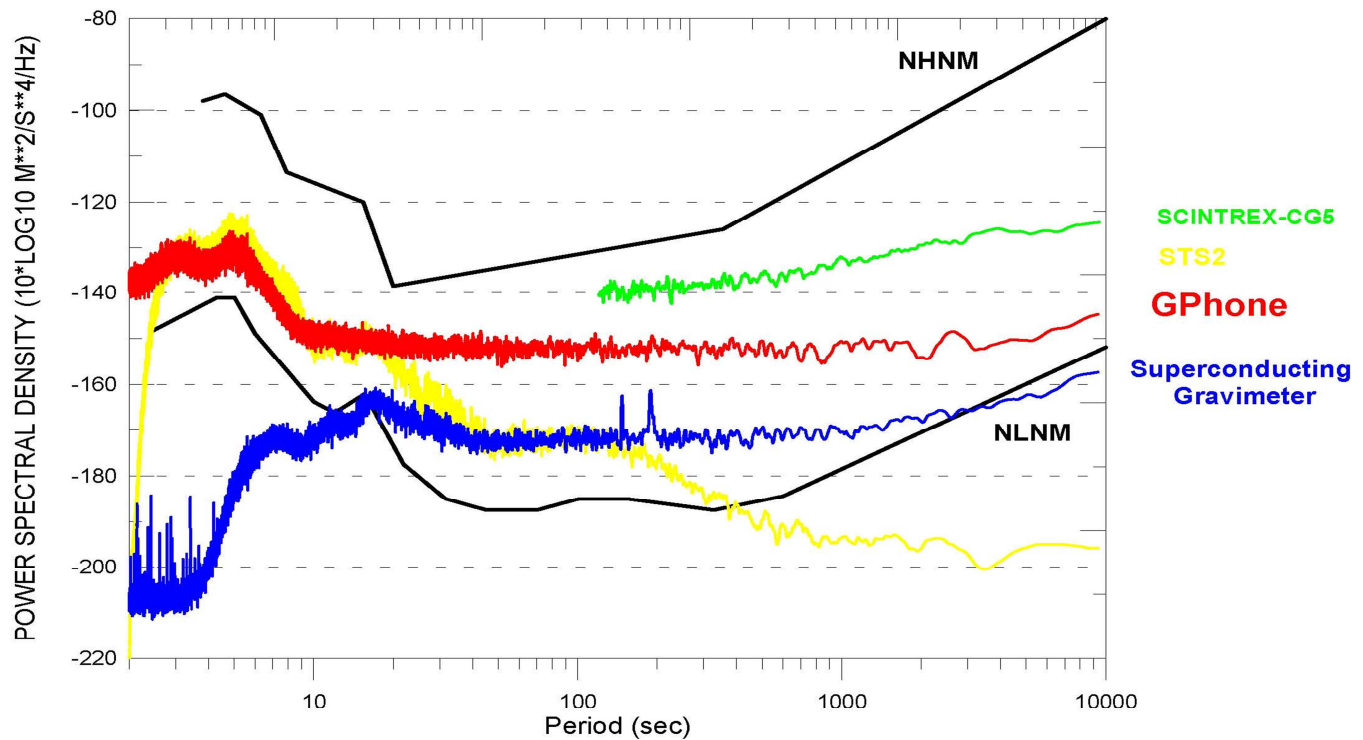
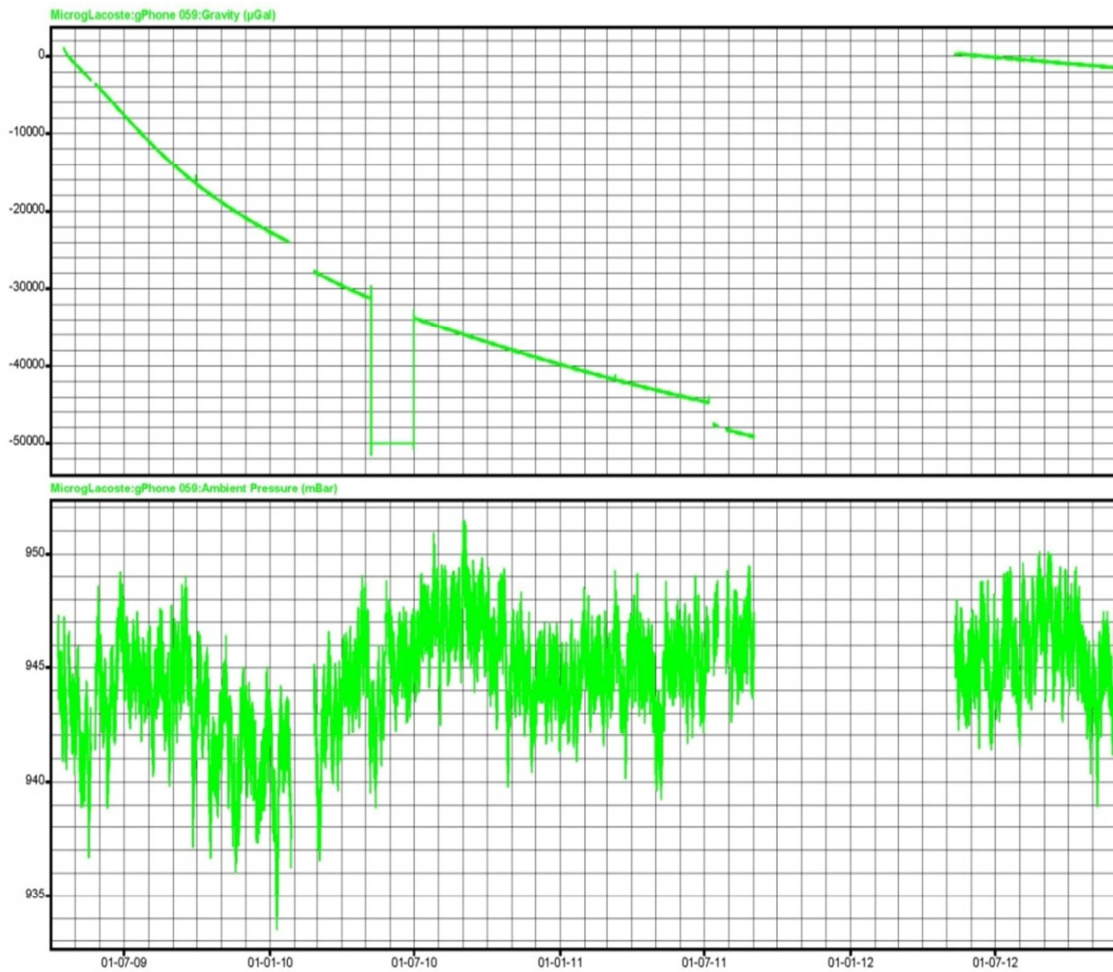


Figure 3. Noise power spectral density (in decibel) of the superconducting gravimeter CT-040, gPhone#32, Scintrex CG5 #010 and a STS-2 broadband seismometer, measured in 2005 in the Walferdange Underground Laboratory for Geodynamics (Luxembourg). It shows the variation of the noises as function of the period as compared to the USGS (Peterson, 1993) low noise model (NLNM) and USGS high noise model (NHNM) with respect to vertical ground acceleration.

3. Observations

We used 940 days of gPhone#59 data from 04-18-2009 to 12-01-2012. The raw gravity and atmospheric pressure data are displayed in Figures 4. There are 33 gaps in the time series due to power outages, very common in Tahiti.



Figures 4. Raw gravity data (top) of the gPhone#059 spring gravimeter and atmospheric pressure observations (bottom), from 04-18-2009 to 12-01-2012, at the vault of Figure 2.

A zoom on the 1-second data (Figure 5) reveals two interesting characteristics of the gravity measurements on an island in the middle of the South Pacific. First, we observe the presence of a huge micro-seismic noise due to the sea swell. It mainly originates from Antarctica with period between 5 s to 25 second with a peak at 10 seconds. In the same figure, we compare with data collected at the same time in a station near Montpellier (South of France) with the gPhone#32 from the University of Luxembourg. The magnitude of the micro-seismic noise in Tahiti is astounding: one cannot even see any tidal signal... Using a low-pass filter, the micro-seismic noise can be eliminated from the raw observations (straight lines in the figure).

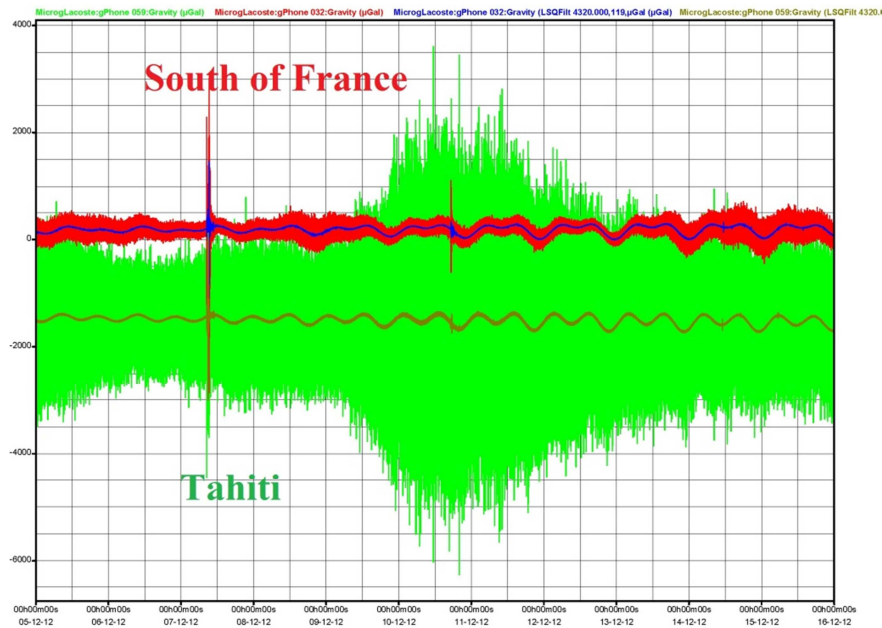
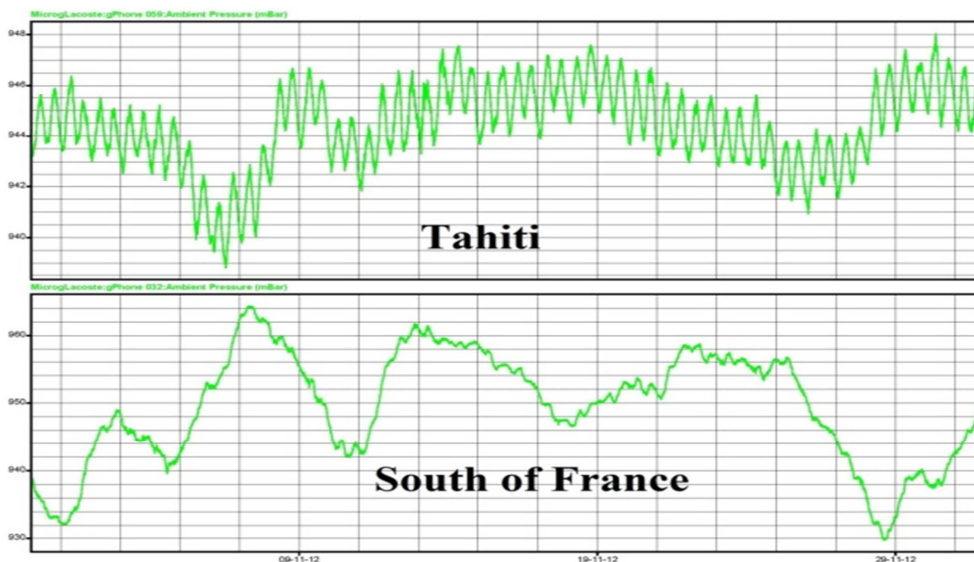


Figure 5. Comparison between the gravity observations in Tahiti (gPhone#59) and in a station near Montpellier in the South of France (gPhone#32). The “green buldge” in the middle of the figure is due to high sea swell around Tahiti during that period.

In Figures 6, we compare the atmospheric pressure data from the two same stations. The strong semi-diurnal signal in the barometric pressure in Tahiti is also striking.



Figures 6. Comparison between the atmospheric pressure recordings in Tahiti and in a station near Montpellier in the South of France.

Table 1. Tidal Parameters at Tahiti-Pamatai estimated using 940-days of observations taken with the gPhone#59 (from 04-18-2009 to 12-01-2012).

Wave	Start frequency /cpd	End frequency /cpd	Amplitude /nm/s ²	Amplitude Factor	Standard Deviation	Phase Lead /degree	Standard deviation /degree
SGQ ₁	0.721499	0.833113	1.636	1.2393	0.0722	0.94	4.14
2Q ₁	0.851182	0.859691	5.287	1.1676	0.0222	2.37	1.27
SGM ₁	0.860896	0.870023	6.434	1.1775	0.0185	0.89	1.06
Q ₁	0.887325	0.896130	40.026	1.1697	0.0029	1.47	0.16
RO ₁	0.897806	0.906315	7.616	1.1717	0.0151	0.98	0.87
O ₁	0.921941	0.930449	208.725	1.1679	0.0005	0.83	0.03
TAU ₁	0.931964	0.940488	2.762	1.1848	0.0412	-4.99	2.36
NO ₁	0.958085	0.966756	16.241	1.1554	0.0058	-0.74	0.33
CHI ₁	0.968565	0.974189	3.151	1.1723	0.0349	-0.40	2.00
PI ₁	0.989048	0.995144	5.505	1.1322	0.0207	0.87	1.18
P ₁	0.996967	0.998028	95.2	1.1448	0.0012	-0.21	0.07
S ₁	0.999852	1.000148	2.218	1.1283	0.0752	-3.86	4.92
K ₁	1.001824	1.003651	285.279	1.1350	0.0004	-0.21	0.02
PSI ₁	1.005328	1.005623	2.16	1.0986	0.0509	5.28	2.93
PHI ₁	1.007594	1.013689	4.221	1.1796	0.0280	-3.41	1.60
TET ₁	1.028549	1.034467	2.98	1.1088	0.0353	0.48	2.02
J ₁	1.036291	1.0448	15.855	1.1280	0.0067	-0.47	0.39
SO ₁	1.064841	1.071083	2.415	1.0356	0.0422	6.90	2.41
OO ₁	1.072583	1.080945	8.626	1.1217	0.0112	-0.96	0.64
NU ₁	1.099161	1.216397	1.677	1.1391	0.0571	2.36	3.27
EPS ₂	1.71938	1.83797	5.953	1.1819	0.0376	0.27	2.15
2N ₂	1.85392	1.862429	20.099	1.1636	0.0118	-0.06	0.68
MU ₂	1.863634	1.872142	24.465	1.1736	0.0098	0.59	0.56
N ₂	1.888387	1.896748	149.738	1.1471	0.0015	1.03	0.09
NU ₂	1.897954	1.906462	28.372	1.1443	0.0080	1.12	0.46
M ₂	1.923765	1.942754	783.127	1.1486	0.0003	1.36	0.02
LAM ₂	1.958232	1.963709	5.838	1.1613	0.0390	2.02	2.23
L ₂	1.965827	1.976926	21.948	1.1389	0.0100	0.69	0.57
T ₂	1.991786	1.998288	21.015	1.1335	0.0108	0.23	0.62
S ₂	1.999705	2.000766	354.057	1.1162	0.0008	1.07	0.10
K ₂	2.00259	2.013689	96.062	1.1142	0.0022	1.21	0.13
ETA ₂	2.031287	2.04739	5.353	1.1105	0.0379	4.16	2.17
2K ₂	2.067579	2.182844	1.411	1.1179	0.1066	3.60	6.11
MN ₃	2.753243	2.869714	3.867	1.1033	0.0156	0.56	0.89
M ₃	2.89264	3.081254	14.249	1.1156	0.0043	-0.15	0.24

4. Tidal analysis

The raw 1-second data (Figures 4) were edited for spikes and other non-tidal disturbances mostly due to earthquakes using Tsoft (van Camp and Vauterin, 2005). The corrected data were then decimated to hourly data by applying a low-pass filter with a cutoff period of 2 hours. An Earth tidal analysis was performed using the ETERNA software (Wenzel, 1996) in which the tidal parameters, the amplitude factor (delta factor) and phase (alpha), were estimated simultaneously with the barometric admittance factor.

The results of the tidal analysis are presented in Table 1. Due to the length of the time series, it was possible to recover 37 tidal waves in the diurnal and semi-diurnal bands. The barometric admittance is $-2.51 \pm 0.15 \text{ nm/s}^2/\text{mbar}$.

5. Discussion

The estimated delta factors for the diurnal and semi-diurnal tides are displayed in Figures 7 and 8. We also corrected the observed tidal parameters for the ocean loading and attraction effects using three different global ocean tides models (Table 2): Schwiderski, FES2004 (Lyard et al., 2006) and CSR3.0 (Eanes and Bettadpur, 1995). Overall, the agreement between the experimental and theoretical tidal factors, hereafter called WDD theoretical model (Dehant et al., 1999), improves with the oceanic loading and attraction effects correction whatever ocean tide models are used. In average, the CSR3.0 model performs the best. The corrected tidal factors are very close to the theoretical values for Q_1 , N_2 and M_2 . The discrepancies for S_2 and K_2 could be due to the strong amplitude of the semi-diurnal signal in the atmospheric pressure or errors in the ocean tides models. A frequency dependent barometric admittance factors may be required for a better correction.

The results in the diurnal band have no apparent sign of any error on the gravimeter calibration factor. The discrepancies in both diurnal and semi-diurnal bands are most likely due to the imperfections in the oceanic loading and attraction calculation. Those affect less the results in the diurnal band as the oceanic loading and attraction is 3 times smaller than in the semi-diurnal band. It is worth to improve the ocean tides maps and methods to compute the direct gravitational attraction of the nearby tidal water masses. One way would be to include local and regional ocean tides maps. As already mentioned, the barometric admittance factor may also play a role in the semi-diurnal band especially for S_2 and K_2 .

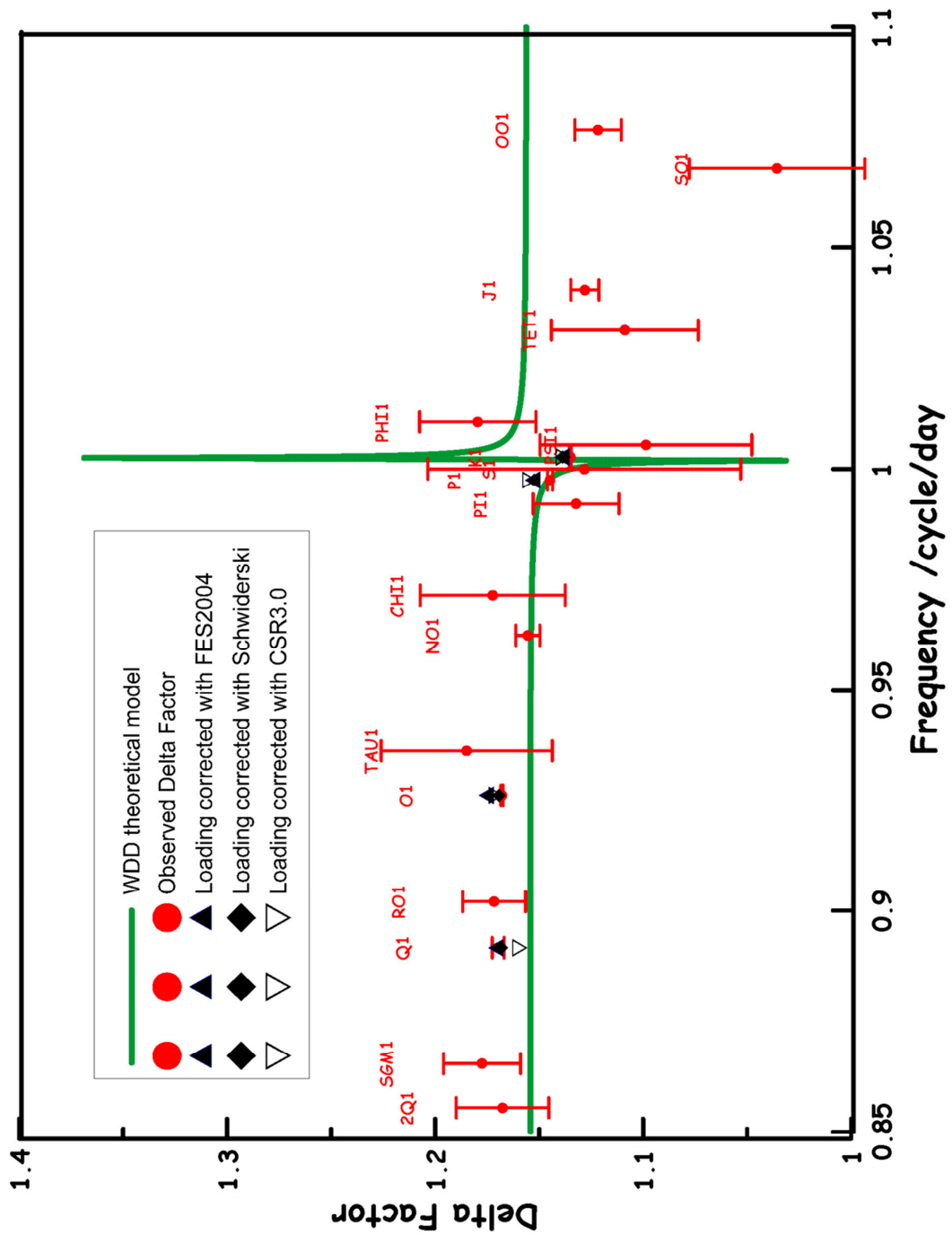


Figure 7. Observed diurnal tidal parameters (red dots). When a tides model is available the observed delta factors are corrected for oceanic loading and attraction (see legend in the figure). The continuous green line represents the WDD Earth tide model.

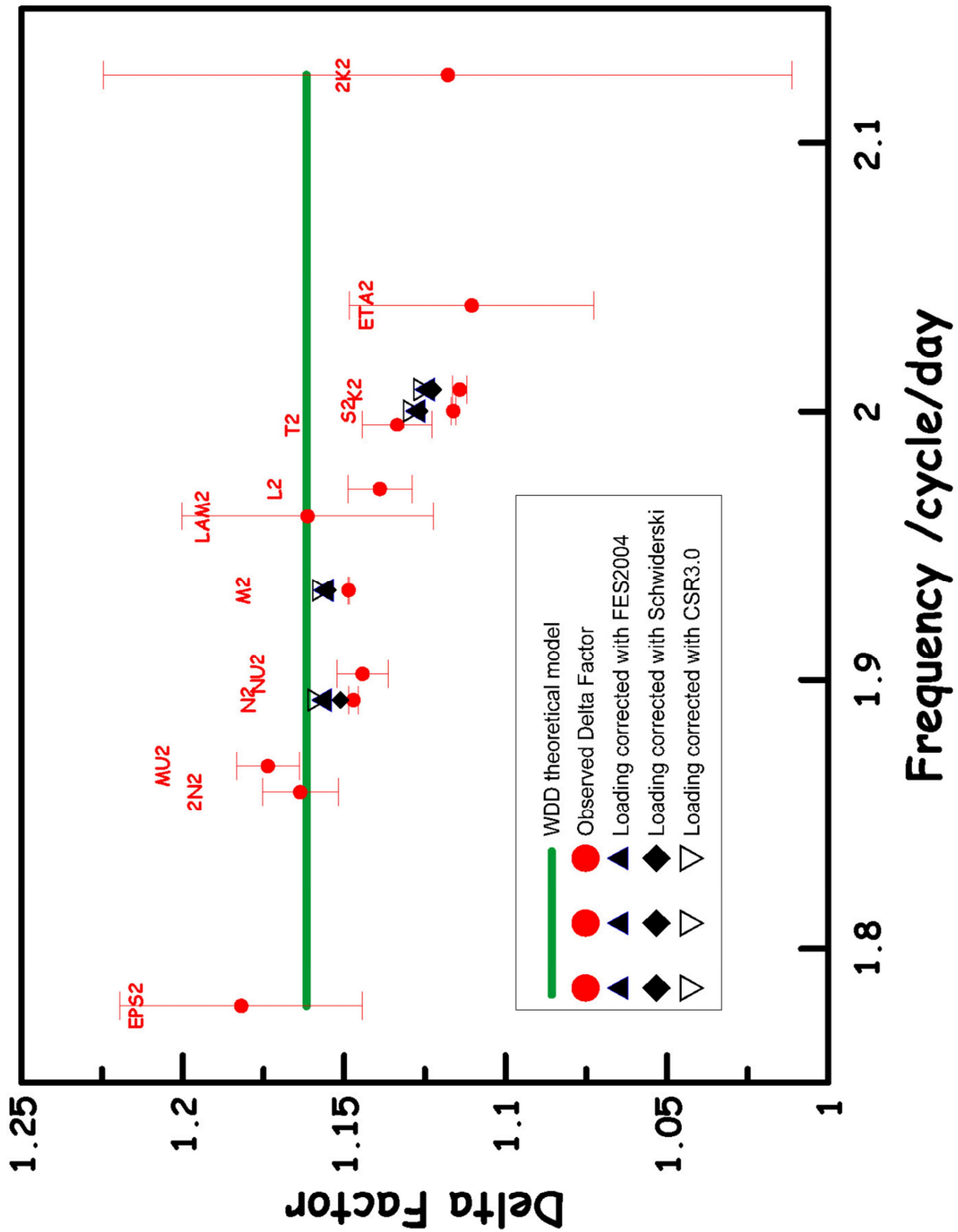


Figure 8. Observed semi-diurnal tidal parameters (red dots). When a tides model is available the observed delta factors are corrected for oceanic loading and attraction (see legend in the figure). The continuous green line represents the WDD Earth tide model.

Table 2. WDD body Earth tides model compared to the observed tidal parameters corrected for the oceanic loading and attraction effects from 3 different global ocean tides models.

Wave	WDD model	Observed tidal parameters corrected for the oceanic loading and attraction effects					
		Schwiderski		CSR3.0		FES2004	
Q ₁	1.1541	1.1681	1.62	1.1593	1.37	1.1695	1.39
O ₁	1.1541	1.1692	0.59	1.1708	0.73	1.1741	0.74
P ₁	1.1493	1.1524	-0.18	1.1546	-0.25	1.1519	-0.19
K ₁	1.1357	1.1387	-0.08	1.1384	-0.31	1.1378	-0.20
N ₂	1.1617	1.1512	0.94	1.1582	0.84	1.1559	0.63
M ₂	1.1617	1.1551	0.79	1.1569	1.10	1.1554	0.93
S ₂	1.1617	1.1266	1.01	1.1287	1.24	1.1269	1.11
K ₂	1.1617	1.1224	1.24	1.1254	1.23	1.1240	1.05

In the ICET data bank (Melchior, 1994), we found the results of the tidal analysis of a previous registration of 163.5 days near the Tahiti-Pamatai site with the LaCoste-Romberg#402 by Ducarme in 1997. In figure 9, the results of 1997 are compared with the results of the gPhone#59 in the diurnal band after corrections for the oceanic tidal loading and attraction effects. The precision of the tidal factors is drastically improved. It also appears that the results of the gPhone#59 are in better agreement with the WDD model. There may be a few explanations: the better calibration of the gPhone#59 by the manufacturer MicrogLaCoste Inc., the duration of our records which is four to five times longer than the previous one in 1997, and the improvement in the hardware and software of the gravimeter.

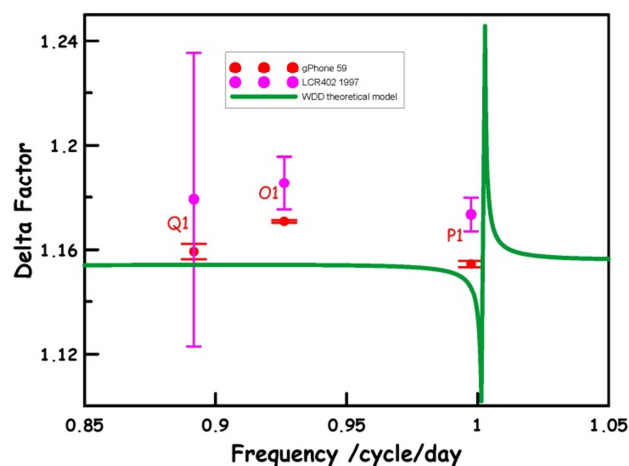


Figure 9. Comparison of the tidal parameters in Tahiti obtained from the LaCoste-Romberg#402 in 1997 and from the gPhone#59, corrected for the ocean tidal loading and attraction effects. The continuous green line represents the WDD Earth tide model.

6. Conclusions

We presented the tidal analysis results of 940 days of gravity measurements with the gPhone#059 in Tahiti. The observations are unique in terms of the presence of an impressive micro-seismic noise and a strong semi-diurnal atmospheric pressure signal. The new observed tidal parameters shows a better fit to the WDD model. However, a comparison with the WDD Earth tides model reveals that the ocean tides loading and attraction effect calculations are very effective for some waves but could still be improved for a few others. Future works will also focus on comparing the measurements of the gPhone with those of the Geoscope seismometers as well as on investigating the observations in terms of loading and hydrology.

Acknowledgments

The gPhone#59 of the Geodesy Observatory of Tahiti was bought in 2008 thanks to funds from the French Space Agency (CNES) and the University of French Polynesia (UPF). It is operated in an isolated vault provided by the French Atomic Energy Agency (CEA) in the high Pamatai valley of Tahiti. This paper was presented during the 17th International Symposium on Earth Tides, “Understand the Earth”, 15-19 April, 2013, Warsaw, Poland.

References

- Clouard V., and Bonneville A., Submarine landslides in Society and Austral Islands, French Polynesia: evolution with the age of edifices in submarine mass movements and their consequences, edited by Locat J., and Mienert J., pp. 335-341, Kluwer Academic Publishers, 2003.
- Dehant V., Defraigne P., and Wahr J.M., Tides for a convective Earth, *J. Geophys. Res.*, 104, B1, 1035-1058, 1999.
- Eanes R.J., and Bettadpur S., The CSR 3.0 global ocean tide model, Technical Memorandum CSR-TM-95-06, Center for Space Research, University of Texas, Austin, Texas, 1995.
- Hildenbrand A., Gillot P.-Y., and Marlin, C., Geomorphological study of long-term erosion on a tropical volcanic ocean island: Tahiti-Nui (French Polynesia), *Geomorphology*, 93,460-481, 2008.
- Lyard F., Lefevre F., Letellier T., and Francis O., Modelling the global ocean tides: modern insights from FES2004, *Ocean Dynamics*, DOI 10.1007/s10236-006-0086-x, 2006.
- Melchior P., A new data bank for tidal gravity measurements (DB92), *Phys. Earth Planet Int.*, 82, 125-155, 1994.
- Peterson J., Observations and modeling of seismic background noise, U.S. Geological Survey, Open-File, report 93-322, 95 pp., 1993.
- Van Camp M., and Vauterin P., Tsoft: graphical and interactive software for the analysis of time series and Earth tides, *Computers in Geosciences*, 31(5) 631-640, 2005.
- Wenzel H-G., The nanogal software: Earth tide data processing package: ETERNA 3.3, *Bulletin d'Information des Marées Terrestres*, 124, 9425-9439, 1996.